Towards Arctic AUV Navigation

Georgios Salavasidis [*,**] **Andrea Munafò** [*]
Catherine A. Harris [*] **Stephen D. McPhail** [*] **Eric Rogers** [**]
Alexander B. Phillips [*]

[*] *National Oceanography Centre, Southampton SO14 3ZH, UK (e-mail: geosal,andmun,cathh,sdm,abp@noc.ac.uk)*
[**] *Department of Electronics and Computer Science, University of Southampton, Southampton SO17 1BJ, UK (e-mail: etar@ecs.soton.ac.uk)*

Abstract:
The navigational drift for Autonomous Underwater Vehicles (AUVs) operating in open ocean can be bounded by regular surfacing. However, this is not an option when operating under ice. To operate effectively under ice requires an on-board navigation solution that does not rely on external infrastructure. Moreover, some under-ice missions require long-endurance capabilities, extending the operating time of the AUVs from hours to days, or even weeks and months. This paper proposes a particle filter based terrain-aided navigation algorithm specifically designed to be implementable in real-time on the low-powered Autosub Long Range 1500 (ALR1500) vehicle to perform long-range missions, namely crossing the Artic Ocean. The filter performance is analysed using numerical simulations with respect to various key factors, e.g. of the sea-floor morphology, bathymetric update rate, map noise, etc. Despite very noisy on-board measurements, the simulation results demonstrate that the filter is able to keep the estimation error within the mission requirements, whereas estimates using dead-reckoning techniques experience unbounded error growth. We conclude that terrain-aided navigation has the potential to prolong underwater missions to a range of thousands of kilometres, provided the vehicle crosses areas with sufficient terrain variability and the model includes adequate representation of environmental conditions and motion disturbances.

Keywords: Arctic AUV navigation, long-range terrain-aided navigation, particle filter

1. INTRODUCTION

As the operation time of under-ice AUV missions increases, the ability to accurately navigate becomes progressively more challenging. Ultra-endurance platforms, such as the ALR1500 (Roper et al. (2017)), which are being developed for performing prolonged operations, can be effectively used under the ice. However, the rapid growth on positioning error and the lack of opportunities for surfacing and obtaining a GPS fix would restrict the range of such platforms. To exploit the long-endurance capabilities requires fit-for-purpose navigation. Although inertial navigation provides sufficient short term accuracy, the performance degrades over time due to sensor errors. To bound the navigation error, approaches include using Long Baseline (LBL), deploying static beacons in the area of interest, or Network LBL (Munafò and Ferri (2017)) where the presence of an underwater sensor network is used to support localisation. If the AUV can be followed at all times, an alternative method relies on using a Ultra-Short Baseline (USBL) mounted on an unmanned surface vehicle (Salavasidis et al. (2016)). A review of relevant background literature is given in Paull et al. (2014). However, in case of polar operations, the thick ice cover prevents surface-based assistance. AUVs operating under ice must entirely rely on on-board sensors and estimation techniques. One possible way to face this challenge is using terrain information (Teixeira et al. (2017)). Given a bathymetric reference map, Terrain-Aided Navigation (TAN) techniques exploit identifiable natural features of the seabed to estimate the vehicle position within this map. Various methods have been reported in the literature to address the TAN estimation problem (Melo and Matos (2017)). One interesting example is reported in (Nygren and Jansson (2004)), where a method for terrain-referencing navigation using a multibeam sonar is proposed. An essential step in this method is to establish that, given dense sonar measurements, the likelihood function is approximately Gaussian and hence the sonar measurements can be fused using a Kalman Filter (KF). When the conditions for using a KF do not hold (even approximately), Particle Filters (PFs) can be effective alternatives (Arulampalam et al. (2002)). One additional constraint for long-endurance missions is that typically the vehicles do not have a large payload capacity, and have limited available computing power (Phillips et al. (2017)). In the case of PFs, this requires a trade-off between the number of parameters to be estimated and computational requirements. The PF complexity problem has seen some research effort by (Teixeira et al. (2017)) using the Marginalized Particle Filter (MPF).

When it comes to Arctic navigation, ice thickness and underwater ice topology might be used as an additional source of information. However, the ice movement makes

this approach very difficult in practise. AUV navigation in Arctic latitudes is even more challenging because of the combined effect of multiple factors: a) limited on-board processing power, b) inability to surface, c) the effect of high latitudes on heading sensors, and d) water currents, which are likely to have the largest impact on the estimation error. This is especially true when the AUV operates mid-water column and/or is not equipped with Doppler-based speed over ground sensors. Consequently the vast majority of the reported AUV missions in the Arctic have been short-term, i.e. lasting from few hours to couple of days. Examples include those reported in Jakuba et al. (2008); Kaminski et al. (2010), where expensive on-board sensors and acoustic-based support systems, which are costly and complex to deploy, are used.

The aim of this paper is to understand the challenges that an AUV will face when operating for months in the Arctic Ocean and to investigate the potential of the TAN to tackle these challenges. To satisfy energy constraints during such a mission, the vehicle is equipped with a limited sensor suite. A low-complexity particle filter is then developed to fuse bathymetric measurements, given a sparse reference map. This is different from the majority of existing research, where high quality sensors and maps are considered. The filter performance is analysed under several environmental condition and with respect to various filter parameters. Simulation results show that the TAN performs significantly more accurately if the AUV is guided over an informative terrain. Therefore, our analysis reveals the importance of proper environmental characterisation before utilising TAN solutions during such long missions.

2. PROBLEM FORMULATION

2.1 ALR1500 & Navigation Sensor Suite

The ALR1500 is a long-endurance 1500m depth rated propeller-driven vehicle developed to accommodate the requirements of the Arctic crossing challenge, having a range in excess of 5000km (Roper et al. (2017)). Such long-endurance is enabled by ensuring low hotel load and slow travel speed ($0.35 - 1$m/s). Given the mission power restrictions, the AUV is equipped with: a Sea-Bird SBE 52-MP Conductivity, Temperature and Depth (CTD) probe, a sensor for deriving the operating depth from the measured hydrostatic pressure; a bespoke low-frequency 4000m range single-beam echo-sounder; and the OCTANS north-seeking Fiber-Optic Gyrocompass (FOG), the only energy expensive sensor, for finding the true north. Although the vehicle is also equipped with an Acoustic Doppler Current Profiler (ADCP), previous field operations have shown that the ADCP might give poor water-relative speed estimates, particularly at depths greater than 1000m, due to a sporadic lack of biological matter to provide back-scatter in clear oceanic water. To avoid poor water-speed estimates and reduce power consumption, the AUV water speed is computed using the propeller RPM calibrated against bottom-relative speed in deep ocean.

Given this sensor suite, there are two main navigation error sources: a) the uncompensated speed for water currents, and b) gyrocompass errors in high latitudes. The heading error depends mainly on the secant of the latitude and the uncertainty in latitude. According to gyrocompass manufactures and the sensor data-sheet (iXblue (2018)), a rough, but pessimistic, estimate of the gyrocompass Root Mean Squared Error (RMSE) is 2°, if the AUV does not exceed 87° of latitude.

2.2 Motion Model

In this paper, localisation is the task of determining the vehicle position. The AUV depth is measured with high update rate from the CTD probe. Given the operating depth and the AUV velocity (compensated for pitch and roll), it can be assumed that the vehicle is levelled horizontally and stabilized in roll and pitch. Given this, the AUV motion model is assumed to be a 2D discrete Markov process:

$$\boldsymbol{x}_k = \boldsymbol{x}_{k-1} + \underbrace{\Delta t \cdot R(\psi_k) \cdot \boldsymbol{u_k}}_{\boldsymbol{\Delta x_k}} + \boldsymbol{m}_k \tag{1}$$

where $\boldsymbol{x}_k = [x_k^N, x_k^E]^T$ is the horizontal vehicle position at time k, expressed in a local North-East (NE) reference frame and $\boldsymbol{m}_k$ is the process noise, which follows $\mathcal{N}(0, \Sigma_m)$. The $\boldsymbol{\Delta x} = [\Delta x^N, \Delta x^E]^T$ represents the vehicle horizontal displacement in NE. To calculate the $\boldsymbol{\Delta x}$, the horizontally-levelled AUV body-frame velocity vector $\boldsymbol{u} = [u^f, u^s]^T$ (containing the forward and starboard speed) is rotated via the rotation matrix R (parametrized only by yaw ψ_k) to the local NE frame and scaled by the sampling time, Δt=1 second.

By getting the expected value of the process model, the AUV can maintain an estimate of its position by Dead-Reckoning (DR). Deep and long-range operations in the Southern Ocean (DynOPO cruise, April 2017) revealed that the DR error for the ALR family of vehicles is of the order of 1% of distance travelled when the AUV operates in bottom-tracking range and is otherwise proportional to the water currents.

2.3 Bathymetric Map and Water Depth Measurement

Typically, before a conventional AUV deployment, the operating area is surveyed and a ship-based bathymetric map is constructed. However, this is not possible in remote, ice covered, areas. The reference map used in this research is obtained from the International Bathymetric Chart of the Arctic Ocean (IBCAO) project (Jakobsson et al. (2012)). This project has created a database of all available bathymetric data north of $64°N$. Constant improvements have led to a grid of 500m resolution. However, only 11% of the Arctic has been covered by multi-beam surveys. This lack of data inevitably causes uncertainty in water-depth estimates. To take into consideration the map uncertainty, it is assumed that the map is affected by $\mathcal{N}(0, \sigma^2_{map})$ noise, and the depth of an arbitrary location is calculated via bilinear interpolation.

The ALR1500 is equipped with a single-beam echo-sounder to measure the vehicle altitude, r_k. If r_k is added to the vehicle depth d_k, the water-depth measurement z_k is obtained. To account for the z_k noise, a noise model $\mathcal{N}(0, \sigma_v^2)$ with intensity that varies with altitude and depth is assumed:

$$\sigma_v^2 = \big(0.25 + (0.0115 \cdot r_k)^2\big) + (5 \cdot 10^{-4} \cdot d_k)^2 \tag{2}$$

where the first term corresponds to the echo-sounder uncertainty (similarly to Claus and Bachmayer (2015)). This term is derived from the 2-σ bound of the maximum acceptable vertical error in sounding sensors for deep bathymetric measurements, according to the S44 International Hydrographic Organization (IHO).The second term corresponds to the depth sensor uncertainty, using the 2-σ bound of the assumed 0.1% maximum error of the measured depth. Given these assumptions, the measurement function is:

$$z_k = h(\boldsymbol{x}_k) + \omega_k \tag{3}$$

where $h(\cdot)$ is the non-linear function that relates the reference map at position $\boldsymbol{x}_k$ to the water-depth measurement z_k. The additive error term $\omega_k \sim \mathcal{N}(0, \sigma_\omega^2)$ is formed as the sum of independent map and measurement noise intensities ($\sigma_\omega^2 = \sigma_{map}^2 + \sigma_v^2$). Therefore, the likelihood function is defined as $p(z_k|\boldsymbol{x_k}) = p(z_k - h(\boldsymbol{x_k})) = p(\omega_k)$.

3. BAYESIAN ESTIMATION

This section outlines the basics behind Bayesian estimation and PFs. For a detailed treatment in a general setting see e.g. Arulampalam et al. (2002) and references therein.

Using the Markov property of the process model (1), Bayes Filters (BF) determine recursively the posterior probability density over the state conditioned on all the available information $p(\boldsymbol{x}_k|z_{1:k})$. When an analytical solution of the BF is not possible, approximate methods can be used. Such method is the Sampling Importance Resampling (SIR) filter, which is used in this paper.

3.1 Sampling Importance Resampling Filter

Let N represent the number of particles and $\boldsymbol{x}_k^i$ be the i-th particle with associated weight w_k^i at time-step k. To successfully track the vehicle, particles must be drawn from the probability density of the current state, also termed a target density. However, such density is not available to be sampled. Instead, the importance sampling principle permits samples to be drawn from an approximation of the target density, called importance (or proposal) density. If arbitrary samples $\boldsymbol{x}_k^i$ are drawn from the appropriately chosen importance density $q(\boldsymbol{x}_k|z_{1:k})$ and the target density $p(\boldsymbol{x}_k|z_{1:k})$ can be evaluated pointwise, then the posterior density can be approximated as:

$$p(\boldsymbol{x}_k|z_{1:k}) \approx \sum_{i=1}^{N} w_k^i \delta(\boldsymbol{x}_k - \boldsymbol{x}_k^i) \tag{4}$$

where δ is the impulse function and w_k^i the normalized importance weight of the $i-$th particle given by (5).

$$w_k^i \propto \frac{p(\boldsymbol{x}_k^i|z_{1:k})}{q(\boldsymbol{x}_k^i|z_{1:k})} \propto w_{k-1}^i \frac{p(z_k|\boldsymbol{x}_k^i)p(\boldsymbol{x}_k^i|\boldsymbol{x}_{k-1}^i)}{q(\boldsymbol{x}_k^i|\boldsymbol{x}_{k-1}^i, z_k)} \tag{5}$$

One possible selection for the importance density is the prior density $q(\boldsymbol{x}_k|\boldsymbol{x}_{k-1}, z_k) = p(\boldsymbol{x}_k|\boldsymbol{x}_{k-1})$. In this case, particles are weighted using only the likelihood density: $w_k^i \propto w_{k-1}^i p(z_k|\boldsymbol{x}_k^i)$. A common problem of this algorithm is the so-called sample impoverishment or degeneracy (Arulampalam et al. (2002)). To mitigate the degeneracy effect, the resampling step has been introduced. When resampling is performed at every time-step, the weights are given by $w_k^i \propto p(z_k|\boldsymbol{x}_k^i)$ and the SIR algorithm is formed.

Algorithm 1 shows a pseudocode of the SIR algorithm. The algorithm receives as input the particles from the

Algorithm 1 Sampling Importance Resampling

$[\{\boldsymbol{x}_k^i\}_{i=1}^N, \hat{\boldsymbol{x}}_k, P_k] \leftarrow$ **SIR** $[\{\boldsymbol{x}_{k-1}^i\}_{i=1}^N, \boldsymbol{\Delta x}_k, z_k]$

1: **for** $i = 1 \rightarrow N$ **do**
2: $\quad \boldsymbol{m}_k^i \sim \mathcal{N}(0, \Sigma_m)$ ▷ Process Noise Sample
3: $\quad \boldsymbol{x}_k^i \leftarrow \boldsymbol{x}_{k-1}^i + \boldsymbol{\Delta x}_k + \boldsymbol{m}_k$ ▷ Particle Propagation
4: $\quad w_k^i \leftarrow p(z_k|\boldsymbol{x}_k^i)$ ▷ Particle Weight
5: $w_k^i \leftarrow \frac{w_k^i}{\sum_{l=1}^N w_k^l}, \; i = 1 \rightarrow N$ ▷ Weight Normalisation
6: $\hat{\boldsymbol{x}}_k \leftarrow \sum_{i=1}^N w_k^i \boldsymbol{x}_k^i$ ▷ Position Estimate
7: $P_k \leftarrow \sum_{i=1}^N w_k^i (\boldsymbol{x}_k^i - \hat{\boldsymbol{x}}_k)(\boldsymbol{x}_k^i - \hat{\boldsymbol{x}}_k)^T$ ▷ Covariance
8: $[\{\boldsymbol{x}_k^i\}_{i=1}^N\}] \leftarrow$ Resampling $[\{\boldsymbol{x}_k^i, w_k^i\}_{i=1}^N\}]$

preceding iteration, the AUV displacement $\boldsymbol{\Delta x}_k$, and the observation z_k. Outputs of the algorithm are the posterior particles and the filter point estimates $\{\hat{\boldsymbol{x}}_k, P_k\}$. Particles are propagated using the process model (1) in step 3. Then, step 4 assigns weights to the particles using the likelihood function. On completion of these steps, the algorithm normalises the weights and calculates the point estimates for this iteration (steps 5-7). Step 8 performs the so-called Systematic Resampling (see Arulampalam et al. (2002) and references therein).

4. SIMULATION SET UP

The TAN algorithm is implemented and evaluated with respect to environmental characteristics and filter parameters. It is assumed that the AUV crosses the Arctic Ocean from Svalbard to the Barrow coast in Alaska ($>$ 3000km), which is a science-driven aspirational use-case, along two morphologically different trajectories, see Fig. 1. The westerly trajectory (black waypoints) defines a less informative path, since the Canada Basin (CB) is a deep and relatively flat oceanic basin. By re-arranging these waypoints to avoid the CB, the eastern path (white waypoints) is formed. Note that both trajectories avoid critical latitudes (red circle centred at 90° of latitude) where the gyrocompass has a large error. At the beginning

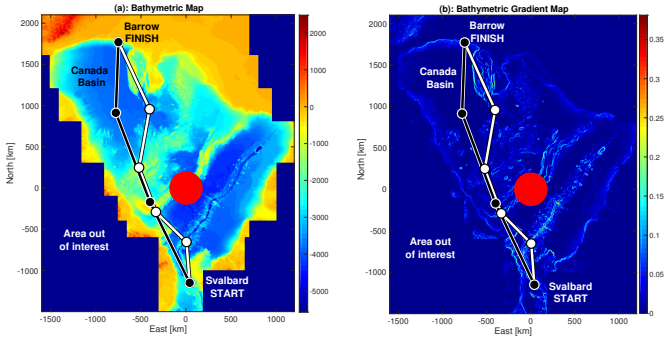

Fig. 1. (a) Bathymetric map with a set of mission waypoints. (b) Bathymetric gradient map. Large errors of gyrocompass - read circle region.

of each run, the AUV is launched near Svalbard. Experiments assume constant 1m/s forward speed and 1500m operating depth, unless the water is shallower and the AUV switches to a fixed (100m) altitude following mode.

Table 1. Parameters Under Consideration

Number of particles, N	$250, 500, 1000, 2000$ $5000, 7500, 10000$
Process noise intensity σ_m, $\Sigma_m = diag(\sigma_m^2, \sigma_m^2)$	$0.1, 0.25, 0.5, 0.75, 1, 1.25$ $1.5, 2, 2.5, 3, 3.5, 4, 5, 6, 7$ [m]
Bathymetric update rate	$10', 30', 1h, 2h, 3h, 4h, 5h, 10h$
Map vertical noise, σ_{map}	$10, 25, 50, 75, 100$ $125, 150, 175, 200$ [m]
Water Current	$-0.4N, 0.4E$ [m/s]

While the AUV is guided between the waypoints, position estimates are computed using both the SIR algorithm and dead-reckoning (see section 2.2).

To introduce a localisation drift, an unobserved bias term of equal magnitude in north and east direction is assumed to affect the motion model (1). This disturbance simulates the combined effect of unobserved water currents and the gyrocompass error at polar latitudes. Arctic Ocean models show that the expected water current drift is lower than 0.05m/s on average, while peaks are of the order of $0.15 - 0.2$m/s and mostly present along the eastern coastline (Madec (2008)). It is assumed for the simulation that the vehicle drifts on average by 0.2m/s in both north and east direction throughout the entire mission. This assumption causes a significantly higher drift, compared to the expected water current drift. Moreover, to incorporate potential gyrocompass errors, the water current magnitude is further increased to 0.4m/s. This extra error is approximately equivalent to a 8° bias heading error (significantly higher to the expected gyrocompass error) and it allows to exercise the filter efficiency, although DR errors will be significantly over-estimated.

For the TAN, the ICBAO grid map is considered as the baseline water-depth and measurements are assumed to be affected by the measurement error model $\mathcal{N}(0, \sigma_v^2)$. To realistically estimate the measurement noise, the noise intensity is calculated based on the noise-corrupted measurements. Since the determination of vertical error in the reference map is a challenging task (Jakobsson et al. (2002)), the algorithm is tested over a wide range of map noise intensities, σ_{map}. Table 1 lists the examined values of all parameters affecting the TAN performance (discussion is provided in the result section).

5. SIMULATION RESULTS

This section analyses the performance of the TAN algorithm with respect to terrain morphology and the parameters shown in Table 1. The effect of each parameter is demonstrated though M=25 Monte Carlo (MC) runs, while the remaining parameters assumed constant and defined based on power constraints. Note, the intention is not to find the optimal parameter set-up but rather to show the importance in understanding the environmental and filter characteristics for developing a real-time system. The filter performance is examined in terms of RMSE accuracy and estimation repeatability among the MC runs. For illustration, the average RMSE and the minimum-maximum error bounds of the MC runs are plotted. Due to the mission complexity, high accuracy localisation is not to be expected and an error bounded within 100km is considered acceptable. This error bound allows the AUV to surface in a safe open water area of the coast of Barrow for recovery, fulfilling the mission objectives.

The filter is first tested with respect to the process noise intensity. Throughout this experiment, the number of particles is N=5000, which is a sufficiently large number to address the 2D estimation problem (Claus and Bachmayer (2015)) and is feasible considering the ALR1500 processor. These particles are always initialised at the beginning of experiments, whilst the vehicle is on the surface, following a normal distribution with mean the GPS position estimate and σ_{GPS}=5m in each direction. In terms of the bathymetric update rate and the noise in the reference map, a reasonably low frequency scheme (1h) is selected and a high vertical map error is introduced (σ_{map}=100m).

The primary role of the process noise is to capture unmodelled system dynamics and sensor errors. Given the process model (1) assumes only random errors, whereas in simulation the vehicle is affected by systematic errors, the assumed zero-mean Gaussian noise model does not hold. Therefore, if the noise intensity is not large enough, the filter is likely to under-estimate the position drift very quickly. This becomes even more severe when the vehicle crosses low informative terrain and TAN position updates are less effective. Recalling also the PF derivation (Section 3), the process noise intensity parametrizes the proposal density, which essentially defines the area where the particles are to be sampled. Therefore, the intensity of the process noise must take into account unmodelled vehicle dynamics and to provide a sufficient, but not too large, particle spread. Avoiding an unnecessarily large process noise intensity is important for mainly two reasons: a) the number of particles might be insufficient to represent the probability distribution over the state, and b) in the presence of terrain similarities the filter may become trapped in local minima. This is verified by the results presented in Fig 2. A low noise intensity, $\sigma_m \in [0.1\text{m}-0.5\text{m}]$, underestimates the positioning drift and also causes the so-called particle collapse (Arulampalam et al. (2002)), while high noise intensity ($\sigma_m \in [6\text{m}-7\text{m}]$) leads the filter to sometimes stick in local minima and hence in large estimation errors. However, as Fig. 2 also shows, it

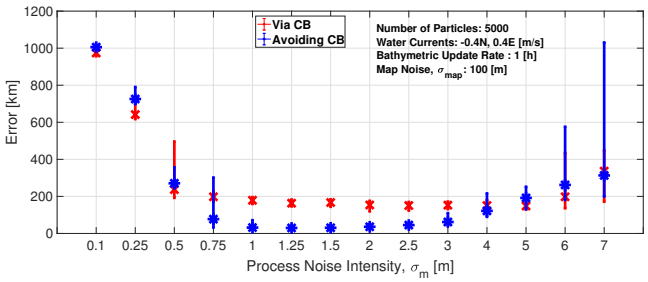

Fig. 2. Average RMSE (crosses/asterisks) and error bounds (error bars) with respect to noise intensity. Red for the trajectory via CB, blue for avoiding CB.

is possible to tune the filter ($\sigma_m \in [1\text{m}-3\text{m}]$) so that the position drift is not underestimated and the filter does not get trapped in local minima. For the subsequent analysis, σ_m=1.5m is selected, although any process noise intensity within the 1m−3m range can be selected. The effect of the terrain morphology on the filter performance is also

visible. For σ_m=1.5m, the average RMSE is 29km when avoiding the CB and 163km when crossing the CB.

Figure 3 shows the effect of the number of particles on the filter performance. As the number of particles increases, experiments that avoid the CB show that the filter provides higher estimation accuracy and repeatability (shown by shorter error bounds among the MC runs). Once all MC runs are convergent, the filter is saturated (in terms of the number of particles) and beyond this point the number of particles does not significantly affect the filter accuracy. In contrast, experiments across the CB show that an increase in the number of particles does not result in an increase in filter performance. This demonstrates that, given a reasonable number of particles, the terrain morphology drives the estimation accuracy. Although N=2000 appears sufficient for both trajectories, N=5000 is selected for the subsequent analysis to assure that the number of particles is sufficient to cover the state space when considering more extreme scenarios (lower bathymetric update rate and higher errors in the map).

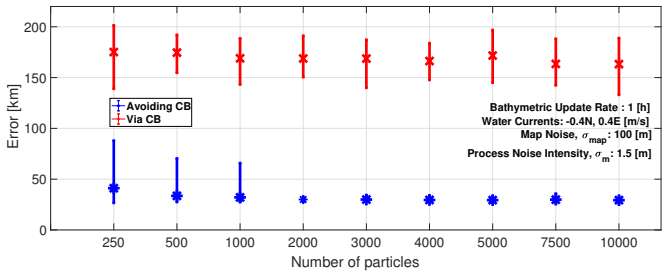

Fig. 3. Average RMSE (crosses/asterisks) and error bounds (error bars) with respect to number of particles.

Figure 4 shows the estimation accuracy and repeatability in terms of the vertical map noise intensity. The increase in the noise intensity results in a reduction in both accuracy and repeatability for both trajectories. However, the navigation error is considered acceptable even in the extreme condition of σ_{map}=200m, when the AUV avoids the CB. Practically, having such large noise in the reference map means that the algorithm relies on extreme terrain variations and massive features.

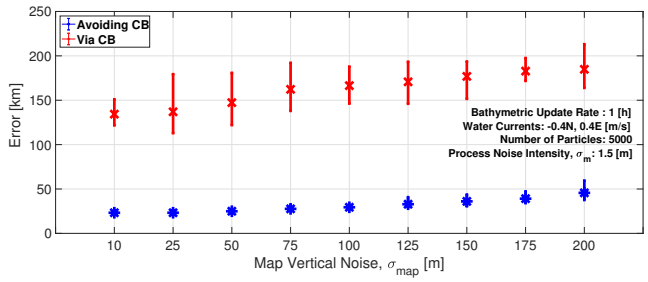

Fig. 4. Average RMSE (crosses/asterisks) and error bounds (error bars) with respect to map vertical noise intensity.

The effect of the sampling frequency is shown in Fig. 5. For these experiments, σ_{map}=100m is selected since this level of noise already heavily distorts the baseline map. As

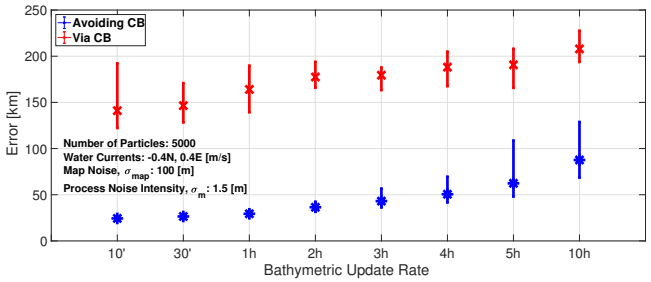

Fig. 5. Average RMSE (crosses/asterisks) and error bounds (error bars) with respect to bathymetric update rate.

the update time increases, the estimation accuracy and repeatability drop for both trajectories. Although significant conservation in power can be achieved by using a very low frequency scheme (e.g. 10h), the low estimation repeatability shows that the filter is less robust and such a low update rate might be risky (potentially leading to vehicle loss under the ice). Given the ALR1500 specification, an update rate of $1h$ does not cause power issues, whist maintaining high accuracy and robustness.

Figure 6 compares the actual vehicle path with the TAN (averaged over the MC runs) and DR estimates over the two considered trajectories. The environmental and filter related parameters are as defined before. For both trajectories, TAN estimates are almost aligned with the actual path before approaching the CB, while DR estimates drift linearly over time due to the simulated motion disturbances. However, once the AUV enters the CB, the TAN error increases because of low terrain-variation (see Fig. 6), whereas the morphologically variable path (avoiding CB) allows the filter to maintain the error below 20km for almost the entire mission. As the location of the mission end forces the AUV to eventually enter a small flat region of the CB, TAN estimates inevitably experience an error increase at this point. The instantaneous RMSE (averaged over all MC runs) at the end of the mission is 91km when not crossing the CB, while by crossing the entire CB is 173km. Given this extreme water currents applied, the corresponding instantaneous DR error is above 1800km.

Figure 7 shows the estimation error with the respective 2-σ confidence bounds in each direction over time. The filter uncertainty is approximated as a normal and uncorrelated distribution (although the posterior distribution is often highly multi-modal). Note that the time-indexed RMSE is almost always within the 2-σ confidence bounds by avoiding the CB, whereas the filter underestimates the positioning error once the vehicle enters the CB.

6. CONCLUSION AND FUTURE WORK

This paper developed and analysed under several conditions the performance of a terrain-aided navigation algorithm during a simulated crossing of the Arctic Ocean with the ALR1500, an ultra-endurance AUV. Given a sparse bathymetric map and computational power constraints, a low dimension particle filter was used to fuse measurements from a limited number of motion sensors and a low-rated single-beam echo-sounder. The effect of various

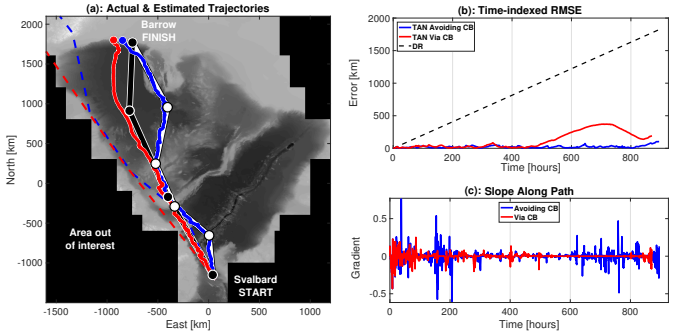

Fig. 6. (a) Actual and estimated path over the two morphologically different trajectories. Blue lines (solid for TAN and dashed for DR) correspond to position estimates while the actual path avoids the CB (white). Red lines (solid for TAN and dashed for DR) correspond to position estimates while the actual path crosses the CB (black). (b) Estimation error for TAN and DR over time and over the two trajectories. (c) Bathymetric slope along the two trajectories.

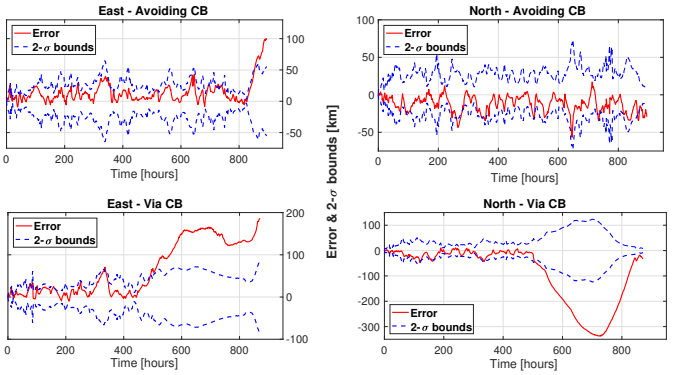

Fig. 7. TAN error in each direction over time and over the two trajectories with the corresponding 2-σ confidence bounds.

parameters on the filter performance was demonstrated along two morphologically different trajectories. Results showed that the algorithm was able to keep the estimation error within an acceptable range, given a sufficiently informative terrain. Future research will focus on three key areas: a) PF robustness (escaping from local minima and divergence detection) and comparisons between non-linear estimators (e.g. Unscented Kalman filter and other PF variants), b) development of a probabilistic bathymetric map of the Arctic Ocean, and c) development of a path planning algorithm for supporting the navigation system. Moreover, to verify our assumptions and prepare for future under-ice work, we have planned a two months deployment in the Atlantic Ocean.

ACKNOWLEDGEMENTS

This work was supported in part by the ROBOCADEMY (FP7 Marie Curie Programme ITN Grant Agreement Number 608096) and the NERC Oceanids Programme.

REFERENCES

Arulampalam, M.S., Maskell, S., Gordon, N., and Clapp, T. (2002). A tutorial on particle filters for online nonlinear/non-Gaussian Bayesian tracking. *IEEE Transactions on signal processing*, 50(2), 174–188.

Claus, B. and Bachmayer, R. (2015). Terrain-aided navigation for an underwater glider. *Journal of Field Robotics*, 32(7), 935–951.

iXblue (2018). OCTANS Fiber-Optic Gyrocompass. `https://www.ixblue.com/products/octans`. Accessed: 2018-03-17.

Jakobsson, M., Calder, B., and Mayer, L. (2002). On the effect of random errors in gridded bathymetric compilations. *Journal of Geophysical Research: Solid Earth*, 107(B12).

Jakobsson, M., Mayer, L., Coakley, B., Dowdeswell, J.A., Forbes, S., Fridman, B., Hodnesdal, H., Noormets, R., Pedersen, R., Rebesco, M., et al. (2012). The international bathymetric chart of the Arctic Ocean (IBCAO) version 3.0. *Geophysical Research Letters*, 39(12).

Jakuba, M.V., Roman, C.N., Singh, H., Murphy, C., Kunz, C., Willis, C., Sato, T., and Sohn, R.A. (2008). Long-baseline acoustic navigation for under-ice autonomous underwater vehicle operations. *Journal of Field Robotics*, 25(11-12), 861–879.

Kaminski, C., Crees, T., Ferguson, J., Forrest, A., Williams, J., Hopkin, D., and Heard, G. (2010). 12 days under ice–an historic AUV deployment in the Canadian High Arctic. In *Autonomous Underwater Vehicles (AUV), 2010 IEEE/OES*, 1–11. IEEE.

Madec, G. (2008). NEMO ocean engine. *Note du Pole de modelisation, Institut Pierre-Simon Laplace (IPSL), France*, 27, 1288–1619.

Melo, J. and Matos, A. (2017). Survey on advances on terrain based navigation for autonomous underwater vehicles. *Ocean Engineering*, 139, 250–264.

Munafò, A. and Ferri, G. (2017). An acoustic network navigation system. *Journal of Field Robotics*, 34(7), 1332–1351.

Nygren, I. and Jansson, M. (2004). Terrain navigation for underwater vehicles using the correlator method. *IEEE Journal of Oceanic Engineering*, 29(3), 906–915.

Paull, L., Saeedi, S., Seto, M., and Li, H. (2014). AUV navigation and localization: A review. *Oceanic Engineering, IEEE Journal of*, 39(1), 131–149.

Phillips, A., Haroutunian, M., Murphy, A.J., Boyd, S., Blake, J., and Griffiths, G. (2017). Understanding the power requirements of autonomous underwater systems, part i: An analytical model for optimum swimming speeds and cost of transport. *Ocean Engineering*, 133, 271–279.

Roper, D.T., Phillips, A.B., Harris, C., Salavasidis, G., Pebody, M., Templeton, R., Vikraman, S.S.A., Smart, M., and McPhail, S. (2017). Autosub Long Range 1500: an ultra-endurance AUV with 6000 Km range. In *MTS/IEEE Oceans'17-Aberdeen*. IEEE.

Salavasidis, G., Harris, C.A., Rogers, E., and Phillips, A.B. (2016). Co-operative use of marine autonomous systems to enhance navigational accuracy of autonomous underwater vehicles. In *Conference Towards Autonomous Robotic Systems*, 275–281. Springer.

Teixeira, F.C., Quintas, J., Maurya, P., and Pascoal, A. (2017). Robust particle filter formulations with application to terrain-aided navigation. *International Journal of Adaptive Control and Signal Processing*, 31(4), 608–651.